Dielectric Permittivity of Eight Gases Measured with Cross Capacitors

J. W. Schmidt[1] **and M. R. Moldover**[1,2]

A four-ring, toroidal cross capacitor was used to measure accurately the relative dielectric permittivity $\varepsilon(p, T)$ of He, Ar, N_2, O_2, CH_4, C_2H_6, C_3H_8, and CO_2. (ε is often called the "dielectric constant.") The data are in the range from 0 to 50°C and, in many cases, extend up to 7 MPa. The accurate measurement of $\varepsilon(p, T)$ required a good understanding of the deformation of the gas-filled capacitors with applied pressure. This understanding was tested in two ways. First, the experimental values of $\varepsilon(p, T)$ for helium were compared with theoretical values. The average difference was within the noise, $\langle \varepsilon_{\mathrm{expt}} - \varepsilon_{\mathrm{theory}} \rangle = (-0.05 \pm 0.21) \times 10^{-6}$, demonstrating that the four-ring cross capacitor deformed as predicted. Second, $\varepsilon(p, T)$ of argon was measured simultaneously on three isotherms using two capacitors: the four-ring capacitor, and a 16-rod cross capacitor made using different materials and a different geometry. The results for the two capacitors are completely consistent, within the specifications of the capacitance bridge. There was a small inconsistency that was equivalent to 1×10^{-6} of the measured capacitances, or, for argon, $3 \times 10^{-5} A_\varepsilon$, where A_ε is the zero-density limit of the molar polarizability $\wp \equiv (\varepsilon - 1)/[(\varepsilon + 2) \rho]$.

KEY WORDS: argon; carbon dioxide; cross capacitor; dielectric constant; dielectric polarizability; ethane; helium; methane; molar polarizability; natural gas; nitrogen; oxygen; propane.

1. INTRODUCTION

Recently, Moldover and Buckley [1] used a toroidal (ring) cross-capacitor to make very accurate measurements of the relative dielectric permittivity

[1] Process Measurements Division, National Institute of Standards and Technology, Gaithersburg, Maryland 20899-8360, U.S.A.
[2] To whom correspondence should be addressed. E-mail: michael.moldover@nist.gov

for helium, argon, nitrogen, methane, and carbon dioxide at $T = 50°C$ and at pressures p up to 7 MPa. Here, we extend the Moldover–Buckley results down to 0°C and we report results of comparable quality for three additional gases: ethane, propane, and oxygen. The combined results may be used to calibrate on-line, capacitance-based instruments that are designed to measure the heating value of natural gas [2]. In addition, the present results are so precise that they reveal minor flaws in published equations of state. Here and below, we refer to the Moldover–Buckley work by the abbreviation "MB;" we refer to the relative dielectric permittivity with the informal name "dielectric constant" and with the symbol $\varepsilon(p, T)$.

In addition to acquiring new data, we rigorously tested our understanding of the MB, four-ring, toroidal cross capacitor by comparing it to a novel 16-rod cross capacitor made using different materials, geometry, and construction techniques. For this test, we measured $\varepsilon(p, T)$ for argon up to 6 MPa using both capacitors on three isotherms. Because both capacitors were exposed to the same gas while they were in the same thermostated bath and were connected to the same pressure gage, this test was insensitive to impurities in the argon and to imperfect measurements of the temperature and pressure. This test was sensitive only to imperfections of the capacitors, the electrical cables, and the capacitance bridge. The data for the two capacitors agreed within the uncertainty of the capacitance bridge. The very small, systematic differences that were detected could be represented by: $\langle \varepsilon_{rod} \rangle - \langle \varepsilon_{ring} \rangle = (0.161 \pm 0.025) \times 10^{-6} \times (p/\text{MPa})$. These differences are equivalent to $3 \times 10^{-5} A_\varepsilon$ of argon, where A_ε is the zero-density limit of the molar polarizability: $\wp = (\varepsilon - 1)/[(\varepsilon + 2)\rho]$.

This work exploits two advantages of well-designed cross capacitors. (1) Cross capacitors are unusually insensitive to the presence of dielectric layers on their electrodes, as demonstrated both theoretically [3] and experimentally [4]. Dielectric layers include permanent oxides, oil deposits and adsorbed layers of gas. (2) The measured pressure dependence of the cross capacitance is consistent with that predicted from measurements of the elastic constants of the capacitor's electrodes. Confirming this, our measured values of $\varepsilon(p, T)$ for helium agreed with theoretical values, within the uncertainties: $\langle \varepsilon_{expt} - \varepsilon_{theory} \rangle = (-0.05 \pm 0.21) \times 10^{-6}$.

Section 2 describes the cross capacitors. Section 3 describes the instruments, materials, and procedures. Section 4 demonstrates that the MB cross capacitor did indeed deform as predicted when subjected to pressure from helium. Section 4 also compares the argon results obtained using the ring and 16-rod capacitors. Section 5 presents the results for the other gases. Section 6 compares some of the present results with data from other laboratories.
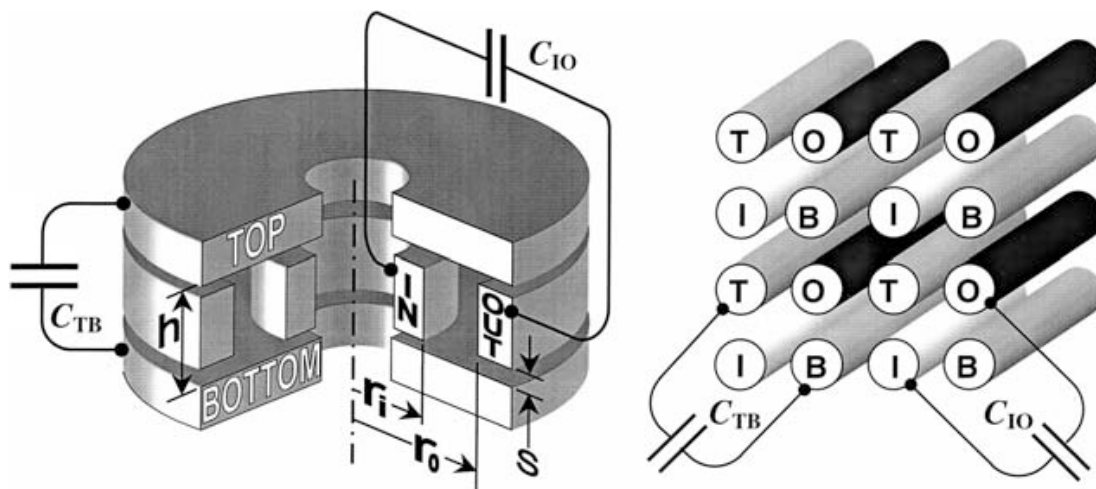
2. CROSS CAPACITORS

2.1. General Remarks

In its conceptually simplest form, a cross capacitor is composed of four, infinitely-long, conducting cylindrical electrodes (in general, not circular cylinders) separated by small, insulating gaps and arranged to form a closed surface [5, 6]. The cross capacitance C_x is the average (with weight w [7]) of the two capacitances measured between opposite pairs of electrodes. In the notation of Fig. 1,

$$C_x \equiv wC_{TB} + (1-w)\,C_{IO}. \tag{1}$$

When cross capacitors are used, there are three conditions that are always implied even if they are not explicitly stated. First, the four cylindrical electrodes are surrounded by a closely fitted, grounded guard so that the capacitance of interest depends upon the "interior" space between the electrodes and is independent of the detailed geometry and the medium outside the electrodes. Second, while C_{TB} is measured, both electrodes of C_{IO} are connected to the grounded guard, and third, while C_{IO} is being measured, both electrodes of C_{TB} are connected to the grounded guard.

Symmetric cross capacitors (defined by $C_{TB} = C_{IO}$ and $w = 0.5$) have a significant advantage in this work. They are comparatively insensitive to

Fig. 1. Sketches of two cross capacitors. For each capacitor, the cross capacitance is $C_x \equiv \frac{1}{2}(C_{TB} + C_{IO})$, neglecting asymmetry. Left: Cut-away view of the ring capacitor. It has two washer-shaped electrodes ("TOP" and "BOTTOM") and two tube-shaped electrodes ("INNER and "OUTER"). Right: The rod capacitor has sets of four rods connected in parallel. (Connections are not shown.). Each set has the same label (e.g., "T"). Each cross capacitor was snugly enclosed by a shield and encased in a pressure vessel.

the presence of dielectric layers on the metal electrodes, such as permanent oxides, a deposited film of pump oil, or an adsorbed gas. For example, if a thin oil layer of thickness t were deposited on an electrode labeled "B" or "Bottom" in Fig. 1, it would simultaneously increase C_{TB} and decrease C_{IO}. In a symmetric case, such a layer would change C_x in proportion to $(t/h)^2$, where h is the distance between opposite pairs of electrodes. In contrast, the same dielectric layer would change the capacitance of a conventional capacitor in proportion to (t/h), and $(t/h) \gg (t/h)^2$ for thin films.

In vacuum, the cross capacitance per meter of length is:

$$C'_x = (\varepsilon_0 \ln 2)/\pi = 1.953\,549\,... \text{ pF} \cdot \text{m}^{-1}, \tag{2}$$

where the electric constant $\varepsilon_0 \equiv 8.854\,187\,817\,... \times 10^{-12}\,\text{F} \cdot \text{m}^{-1}$. Thus, typical values of C_x are on the order of 1 pF. This is a disadvantage because accurate measurements of capacitances on the order of 1 pF require a sophisticated bridge. There are two other disadvantages. Cross capacitors are more complicated to manufacture than other capacitors because they must have at least four electrodes, each of which must be insulated from every other electrode and from the guard. Finally, an array of very well shielded switches is required to connect each electrode pair first to the bridge while its capacitance is being measured and then to ground while the capacitance of the other pair is being measured.

2.2. Ring Cross Capacitor

Except for an important consistency test, the cross capacitor used in the present work was described by MB in detail; it is sketched on the left side of Fig. 1. We call this capacitor the "ring capacitor" and denote its cross capacitance by C_{ring}. The ring capacitor was composed of four rings, i.e., circular, cylindrical electrodes, each having a rectangular cross section. The four electrodes were arranged coaxially to enclose a toroidal volume with a nearly square cross section. The two electrodes designated "top" and "bottom" were shaped like washers. The two electrodes designated "inner" and "outer" were tube-shaped. All four electrodes were made from superinvar, an alloy chosen for its very small coefficient of thermal expansion. Sapphire balls were used to insulate the electrodes from each other and to support the bottom electrode on a grounded, superinvar base. The electrodes were surrounded by a grounded aluminum guard that was separated from the top electrode by sapphire balls. The electrodes and the guard were enclosed by a pressure vessel.

The sapphire balls and superinvar electrodes were assembled into a kinematically stable structure. Three radial "V" grooves were electro-discharge machined into the top and bottom electrodes, and three mating cavities were electro-discharge machined into the inner and outer electrodes. The electrodes and balls were held together by springs; thus, there was very little stress on the rings.

The average radius of the ring capacitor was: $r \equiv (r_o + r_i)/2 \approx 50$ mm. Because of manufacturing errors, the cross section deviated from a square; it had the height $h \approx 9.5$ mm and the width $\Delta r \equiv (r_o - r_i) \approx 10$ mm. The deviation from symmetry is measured by the parameter $\delta \equiv (\Delta r - h)/h \approx 0.05$. Theory [8] has provided several useful results for toroidal cross capacitors with nearly square cross sections, These results include:

$$C_{\text{ring}} = 2 \ln 2 r \varepsilon_0 \varepsilon f(h/r, s/h, t/h, \delta)$$

$$f(h/r, s/h, t/h, \delta) = 1 + e_1(h/r)^2 + e_2(s/h)^2 + e_3(t/h)^2 + e_4\delta^2 + \cdots,$$

(3)

where the coefficients $e_1 = -0.04042$, $e_2 = -0.0017$, and $e_4 = 3.454$. We are not aware of a calculation of e_3 for the ring capacitor; we use results for another geometry to estimate $e_3 \sim 0.035(1 - 1/\varepsilon_f)^2$, where ε_f is the relative permeability of the dielectric film [3]. As expected from Eq. (3), we found that $C_{\text{TB}} \approx 0.72$ pF and $C_{\text{IO}} \approx 0.52$ pF in vacuum. We used Eq. (3) to choose the weight $w = 0.4476$ in Eq. (1) such that $(\partial C_{\text{ring}}/\partial \delta) = 0$. With this choice, C_{ring} was not affected, within the uncertainty of the measurements, by the small movements of the top or bottom electrodes with respect to the inner and outer electrodes that occurred when pressure was applied.

With the asymmetric weighting of C_{TB} and C_{IO}, the cross capacitance depends, in the first order, only on the average radius $r = (r_o + r_i)/2$ of the tori. This average is determined solely by the inner radius of the outer electrode and the outer radius of the inner electrode. Because each electrode was cut out of a single piece of superinvar and because each was subject to very small external forces from springs, gravity, and buoyancy, we expected that the pressure and temperature dependences of r and C_{ring} would be those of superinvar alone. This was confirmed by MB, and additional confirmation appears in Section 3 later.

2.3. Rod Cross Capacitor

As described in Section 4, the rod capacitor was used to test for possible problems in the ring capacitor and the capacitance bridge. The rod capacitor is sketched on the right side of Fig. 1 and in greater detail in Fig. 2. It was composed of 16 Type 303 stainless-steel "rods." Each rod

was a circular cylinder with a length $L = 101.6$ mm and a diameter $D = 9.525$ mm. The rods were arranged parallel to each other in a square array such that each rod was separated from its nearest neighbors by (0.30 ± 0.05) mm. The rods were bolted to a base plate made of the same alloy; however, sapphire washers (6.35 mm in diameter, 0.15 mm thick) and ceramic bushings insulated the rods and the bolts from the base plate. Electrically, the rods were connected in parallel in equivalent groups of four, as indicated by the labels in Fig. 1.

The array of rods was snugly enclosed by a guard electrode. The guard was composed of the base plate, a top plate, and a thick-walled, circular, stainless-steel cylinder. The cylinder surrounded the rods and was bolted to the base plate. A narrow gap separated the cylinder from the top plate of the guard. The top plate of the guard was bolted to one of the four, electrically equivalent, sets of four rods. The top plate was insulated from the bolts by sapphire washers and ceramic bushings.
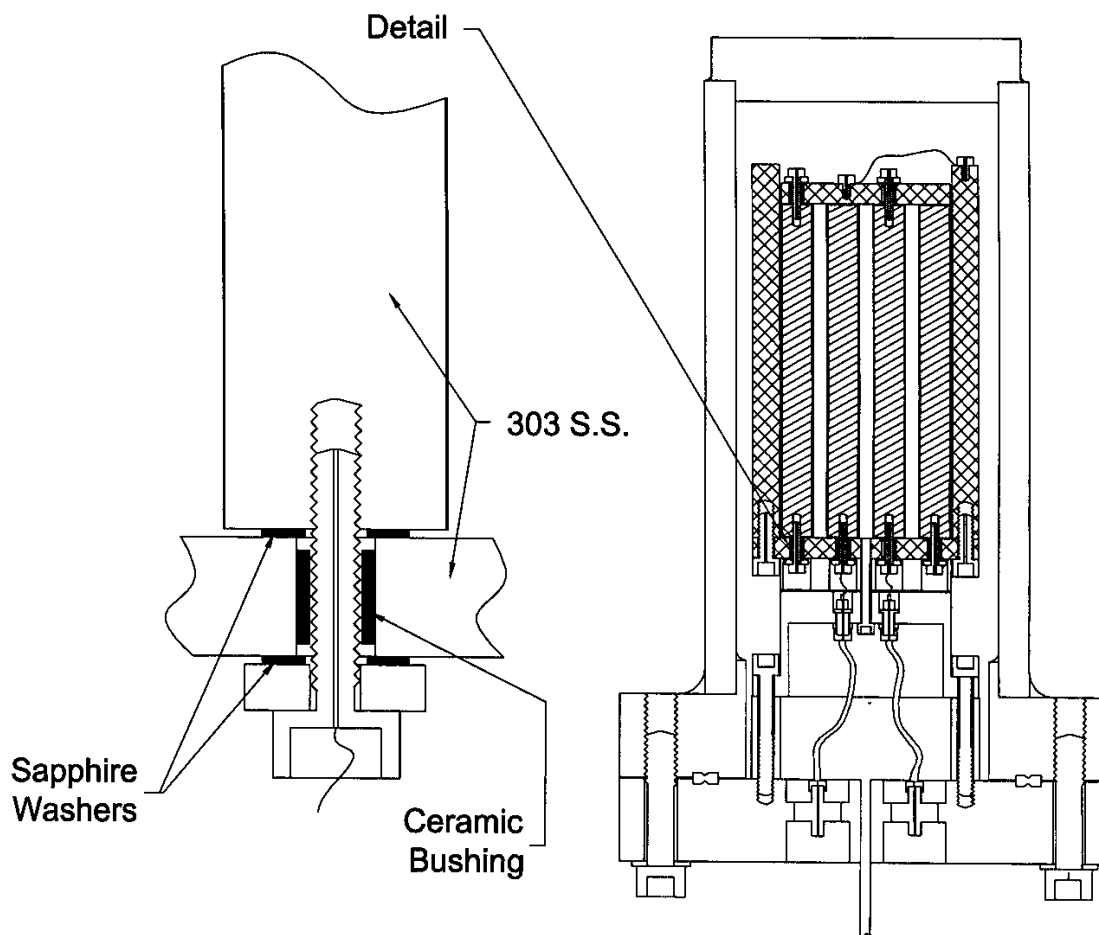

Fig. 2. Scale drawing of section of the rod cross capacitor within its pressure vessel. The rods are hatched; the guard electrode is cross-hatched. The detail drawing shows the sapphire washers and ceramic bushing that insulated the rods from the guard.

In the 16-rod array, there are 9 instances where pairs of rods labeled "T" and "B" can "see" each other across a gas-filled space that is not shielded either by the guard or by the rods labeled "I" or "O." Because there are 9 such pairs we expected that its cross capacitance C_{rod} would be 9 times larger than the cross capacitance of a four-rod array described by Eq. (2); i.e., we expected $C_{rod} = 9C'_x L$ and this was confirmed by the results under vacuum: $C_{TB} = 1.848$ pF and $C_{IO} = 1.813$ pF. Because $C_{rod} \approx 3C_{ring}$, the capacitance measurements could be made with a significantly better signal-to-noise ratio. Electrically, the rod capacitor was more nearly symmetrical than the ring capacitor. ($C_{TB}/C_{IO} = 1.02$ for the rods; $C_{TB}/C_{IO} = 1.39$ for the rings.). We assumed that the small asymmetry resulted from construction errors that left the T and B rods closer together, on the average, than the I and O rods. We modeled this error and chose the weight $w = 0.492$ to use in Eq. (1) so that C_{rod} would be insensitive to small changes in the asymmetry.

There are two reasons why we thought that C_{rod} might be less stable than C_{ring}. First, the electrical lengths of the 16 rods were determined by the distances between the base plate and the top plate in the vicinity of each rod. These distances were determined by the lengths of the four corner rods, the thicknesses of the sapphire washers at both ends of each corner rod, the shapes of the plates and any stresses that happened to be present in this kinematically over-determined structure. (In contrast, C_{ring} was determined by the average radius $r = (r_o + r_i)/2$, and only small forces were applied to the rings.) Second, if a dielectric layer of thickness t (e.g., vacuum pump oil) formed on either the top plate or the base plate of the rod capacitor, it would change C_{rod} fractionally on the order of $(t/L)(1-1/\varepsilon_f)$. (In contrast, a similar layer on an electrode of the symmetrical ring capacitor would change C_{ring} fractionally on the order of $(t/h)^2 (1-1/\varepsilon_f)^2$, which is much smaller for small plausible values of t.) Consistent with our concerns, we found that C_{rod} increased at a rate of 6 ppm/year under vacuum while C_{ring} drifted (0.7 ± 0.9) ppm/year. (1 ppm $\equiv$ 1 part in 10^6.)

2.4. Deformation of Cross Capacitors Under Pressure

As an elastic solid comes into equilibrium under a hydrostatic pressure p, its volume decreases by the factor $k_T p$, where $k_T \equiv -(\partial V/\partial p)_T/V$ is the isothermal volumetric compressibility of that solid. If the solid were isotropic, all its linear dimensions decreased by the factor $k_T p/3$. In this work $p \leqslant 7$ MPa, and the fractional volume changes were $\leqslant 7 \times 10^{-5}$. Buckley et al. [9] applied this idea to the ring capacitor. They noted that applying pressure to the sapphire balls decreased the insulating gaps

$[s \approx 0.15 \text{ mm}$, Fig. 1] between the superinvar rings. By using Eq. (3), they showed that this deformation had a negligible effect on C_{ring} in comparison with the shrinkage of the radii of the inner and outer rings that determine C_{ring}, in the lowest order. For the ring capacitor, their working equation for $\varepsilon_{\text{expt}}$ is

$$\varepsilon_{\text{expt}}(p) = \frac{C_x(p)}{C_x(0)} (1 + k_T p/3). \tag{4}$$

where the value $k_T = (9.43 \pm 0.38) \times 10^{-12} \text{ Pa}^{-1}$ was measured for superinvar samples [9]. To illustrate the importance of the term $k_T p/3$, we shall compare it to A_ε. To do so, we substitute the right hand side of Eq. (4) into the expansion of the molar polarizability as a function of density:

$$\wp(\rho, T) = \left(\frac{\varepsilon - 1}{\varepsilon + 2}\right)\frac{1}{\rho} = A_\varepsilon(1 + b\rho + c\rho^2 + \cdots), \tag{5}$$

where b and c are dielectric virial coefficients. We eliminate the density using the virial equation of state,

$$p = \rho RT(1 + B\rho + C\rho^2 + D\rho^3 + \cdots), \tag{6}$$

where B, C, and D are the density virial coefficients and $R = (8.314472 \pm 0.000015) \text{ J} \cdot \text{mol}^{-1} \cdot \text{K}^{-1}$ is the molar gas constant. Finally, we expand $C_x(p)/C_x(0)$ in powers of $p/(RT)$ to obtain:

$$\frac{C_x(p)}{C_x(0)} = 1 + a_1\left(\frac{p}{RT}\right) + a_2\left(\frac{p}{RT}\right)^2 + \cdots$$

$$a_1 = 3(A_\varepsilon - k_T RT/9) \tag{7}$$

$$a_2 = 3A_\varepsilon(-B + b + A_\varepsilon - k_T RT/3) + (k_T RT/3)^2$$

In the coefficient a_1, the molar polarizability A_ε is "corrected" by the amount $k_T RT/9 = (2.81 \pm 0.11) \times 10^{-3} \text{ cm}^3 \cdot \text{mol}^{-1}$. For helium, $A_\varepsilon \approx 0.517 \text{ cm}^3 \cdot \text{mol}^{-1}$; thus the correction for elastic deformation is 0.54% of A_ε and its uncertainty is 0.02% of A_ε. For methane ($A_\varepsilon \approx 6.55 \text{ cm}^3 \cdot \text{mol}^{-1}$) this correction is 0.043% of A_ε. For gases and pressures considered in this work, $a_2[p/(RT)]^2 \ll a_1[p/(RT)]$. In Section 5.2, we consider the effects of the terms of the coefficient a_2.

Moldover and Buckley tested the isotropic, elastic deformation model for the ring capacitor by measuring $C_{\text{ring}}(p = 0, T)$ and $C_{\text{ring}}(p, T)$ under helium at 50°C. They compared their results with the theoretical values of

$\varepsilon(p)$ based on *ab initio* results from quantum mechanics for the dominant terms. In Fig. 3, we show the MB results at 50°C and our new results at 29 and 0°C. The average difference between the data and the model is surprisingly small: $\langle \varepsilon_{\text{expt}} - \varepsilon_{\text{theory}} \rangle = -0.05 \times 10^{-6}$; the standard deviation of the differences is 0.21×10^{-6}. We expected the average difference to be larger because the uncertainty of k_T is equivalent to 0.45 ppm when averaged from 0 to 7 MPa and because the uncertainty claimed by the manufacturer of the capacitance bridge is "accuracy of 3 ppm." Evidently the bridge can measure capacitance ratios much more accurately than 3 ppm.

In order to prepare Fig. 3, we computed $\varepsilon_{\text{expt}}(p, T)$ using Eq. (4). At each value of the pressure where $C_{\text{ring}}(p, T)$ was measured, we also computed $\varepsilon_{\text{theory}}(p, T)$ by numerically eliminating the density from Eqs. (5) and (6). To implement this procedure, we used the values of A_ε, $B(T)$, $C(T)$,
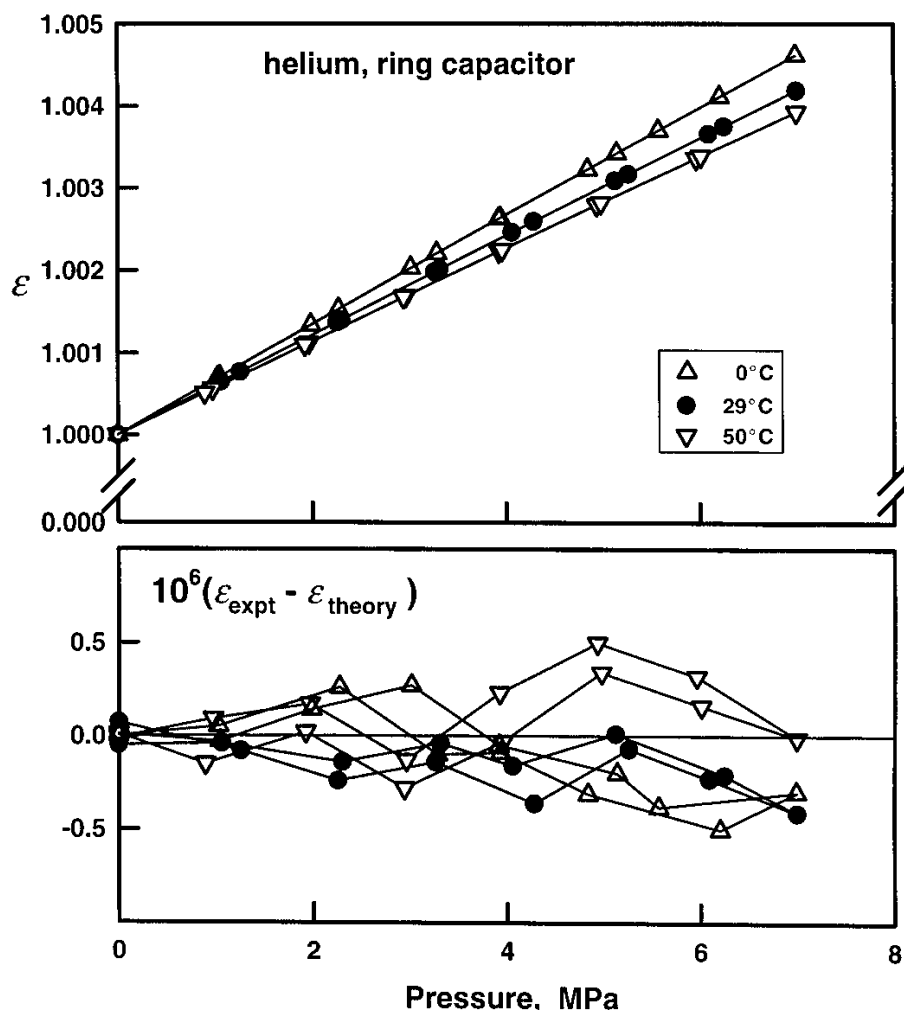

Fig. 3. Differences between the calculated dielectric constant of helium and that measured using the ring cross capacitor. The average difference was $\langle \varepsilon_{\text{expt}} - \varepsilon_{\text{theory}} \rangle = -0.05 \times 10^{-6}$ and its standard deviation was 0.21×10^{-6}. This comparison is absolute; there are no fitted parameters.

$D(T)$, b, and c recommended by MB for helium. To describe the sensitivity of $\varepsilon_{\text{theory}}(p, T)$ to the uncertainties of the recommended values, we list the fractional change in $\varepsilon_{\text{theory}}(7\,\text{MPa}, 323\,\text{K})$ upon increasing each property by its uncertainty: A_ε, 0.06 ppm; B, 0.24 ppm; C, 0.07 ppm; D, 0.01 ppm; b, -0.10 ppm; c, 0.00 ppm. The fractional change in $\varepsilon_{\text{expt}}(7\,\text{MPa}, 323\,\text{K})$ upon increasing k_T by its uncertainty is 0.89 ppm.

We also tested the assumption that the rod capacitor deformed isotropically under pressure. We did not measure the elastic constants of the steel rod stock that was used to make the rods. Instead, we adjusted k_T so that the average $\langle \varepsilon_{\text{expt}} - \varepsilon_{\text{theory}} \rangle$ was approximately zero along two helium isotherms near 0 and 23°C. The resulting value of k_T was $6.8 \times 10^{-12}\,\text{Pa}^{-1}$; it is close to the value $6.4 \times 10^{-12}\,\text{Pa}^{-1}$ that we calculated from handbook values of the elastic constants of Type 303 stainless-steel. The deviations from the fit of k_T are shown in Fig. 4e. If we had used the handbook value of k_T, the deviations would have sloped downward and reached 0.7 ppm at $p = 5\,\text{MPa}$. These deviations are well within the specification "accuracy of 3 ppm" claimed by the manufacturer of the capacitance bridge.

3. INSTRUMENTS, MATERIALS, AND PROCEDURES

For the present work, we used exactly the same cross capacitor and pressure vessel that MB described in detail in Ref. 1. We also used the same capacitance bridge, cables, thermometers, and pressure measuring instruments. For our first measurements (at 29°C) the capacitor was immersed in the same oil bath described by MB. However, a better oil bath manufactured by Hart Scientific Co.[3] became available. In the better bath, the steady temperature gradients and the temperature fluctuations were both less than 0.5 mK. The bath temperature was measured with a calibrated standard platinum resistance thermometer. We believe that the present data on the isotherms at 40, 23, and 0°C have a temperature uncertainty of less than 2 mK with respect to the International Temperature Scale of 1990 (ITS-90). MB estimated that the uncertainty of the pressure measurements was "the quadrature sum of three terms: $30 \times 10^{-6}p$ from the uncertainty of the standard, 55 Pa from changes of the calibration function between calibrations, and 64 Pa from the rms deviations of readings from the calibration functions. We represent this uncertainty as: $(3 \times 10^{-5}p + 84\,\text{Pa})$."

---

[3] In order to describe materials and experimental procedures adequately, it is occasionally necessary to identify commercial products by manufacturer's name or label. In no instance does such identification imply endorsement by the National Institute of Standards and Technology, nor does it imply that the particular product or equipment is necessarily the best available for the purpose.

Whenever gas was admitted into (or withdrawn from) the pressure vessel enclosing the cross capacitor, the average temperature of the capacitor increased (or decreased) and then, the capacitor returned to equilibrium. The late stage of the $C_{ring}(p, T)$ vs. time record was fit by an exponential decay with the time constant $\tau_{thermal}$. The improved oil bath enabled us to measure $\tau_{thermal}$ accurately. For the ring capacitor, $\tau_{thermal} = 7\,h$ under vacuum; $\tau_{thermal} = 0.8\,h$ in argon; and, $\tau_{thermal} = 0.2\,h$ in helium. Under similar conditions, $\tau_{thermal}$ of the rod capacitor was approximately 20% longer than $\tau_{thermal}$ of the ring capacitor. Once $\tau_{thermal}$ had been determined for each gas, we adopted the protocol of measuring $C_x(p, T)$ during the interval $2 \times \tau_{thermal}$ following each pressure change and extrapolating to infinite time. Because of this protocol, the hysteresis in the present $\varepsilon(p, T)$ tables is smaller than that reported by MB.

In future work, we shall avoid capacitance measurements under vacuum where $\tau_{thermal}$ is so long. Instead, to speed data collection, we will measure $C_x(p, T)$ on isotherms down to pressures on the order of 0.1 MPa and we will determine the vacuum capacitance $C_x(p = 0, T)$ by fitting to $C_x(p, T)$ or $C_x(\rho, T)$.

All the test gases were used as purchased. The helium, argon, nitrogen, and methane used in this work were withdrawn from the same cylinders as the gases used in Ref. 1. For this work, we purchased ethane, propane, oxygen and a purer sample of CO_2 than that used in Ref. 1.

The ethane was purchased from Air Products & Chemicals, Inc.[3] The vendor specified that the ethane had "99.999% minimum purity" by volume. The vendor also specified upper bounds, by volume, for specific impurities: $N_2 < 3 \times 10^{-6}$; $O_2 < 1 \times 10^{-6}$; $CO/CO_2 < 2 \times 10^{-6}$; and $H_2O < 3 \times 10^{-6}$. The propane was purchased from Matheson Gas Products. The vendor specified that the propane had "99.993% minimum purity" by volume. The vendor also specified upper bounds, by volume, for specific impurities: $CH_4 < 1 \times 10^{-6}$; $C_2H_6 < 20 \times 10^{-6}$; $C_2H_4 < 5 \times 10^{-6}$; $n\text{-}C_4H_{10} < 5 \times 10^{-6}$; $i\text{-}C_4H_{10} < 20 \times 10^{-6}$; $N_2 < 3 \times 10^{-6}$; $O_2 < 1 \times 10^{-6}$; $CO < 2 \times 10^{-6}$; $CO_2 < 1 \times 10^{-6}$; and $H_2O < 2 \times 10^{-6}$. The carbon dioxide was purchased from Air Products & Chemicals, Inc. The vendor described the gas as "SFC/SFE Grade $> 99.9999\%$" and specified the water content as $< 0.25 \times 10^{-6}$ by mole fraction. We took the same precautions to avoid contaminating the test gases that MB did.

In dielectric studies, water vapor is a particularly obnoxious impurity because its molar polarizability is comparatively large; for water vapor near 0°C, $A_\varepsilon \approx 79\ cm^3 \cdot mol^{-1}$. If the gases used in this work contained as much water as the vendor's specification permitted, the effect of the water on the measured value of A_ε would be smaller than the effect of the uncertainty of the pressure measurements.

Each measurement cycle began with the capacitor evacuated. Typically, the pressure was raised in 1 MPa steps up to 7 MPa and then lowered in 1 MPa steps. Following each pressure change, an interval of 3 to 7 h elapsed to allow the capacitor to approach thermal equilibrium. Thus, a complete cycle of 12 steps took several days. With each test gas, at least two complete measurement cycles were conducted. The data from the last cycle are reported in Tables II and III. However, no significant differences between the last two cycles were ever detected.

4. CONSISTENCY TEST: RING AND ROD CAPACITORS IN ARGON

The accuracy of $\varepsilon(p, T)$ obtained from the ratios $C_x(p, T)/C_x(0, T)$ depends upon the linearity of the capacitance bridge in two, very narrow, portions of its operating range. All of the values of $\varepsilon(p, T)$ reported in this work use capacitance measurements with sub-ppm resolution in the ranges $0.518 \text{ pF} < C_{TB} < 0.552 \text{ pF}$ and $0.718 \text{ pF} < C_{TB} < 0.764 \text{ pF}$. Our ability to test the accuracy of the system {ring capacitor + bridge} within these narrow ranges is quite limited. The comparison of the helium data with theory (Fig. 3) is a very strong test of absolute accuracy in the very small sub-ranges spanned by the helium data ($0.518 \text{ pF} < C_{TB} < 0.520 \text{ pF}$ and $0.718 \text{ pF} < C_{TB} < 0.721 \text{ pF}$). The accuracy of the system was also tested by MB when they compared their values of $\varepsilon(p, T)$ for Ar, N_2, CH_4, and CO_2 with the values of $\varepsilon(p, T)$ obtained in other laboratories. However, such comparisons cannot be used to argue that the present system is more reliable than the conventional capacitors used in other laboratories. Therefore, we made a powerful consistency test that compared the ring and rod capacitors. In effect, the test compared the linearity of the bridge in the low ranges mentioned above to the linearity of the same bridge in the range $1.74 \text{ pF} < C_{TB} < 1.80 \text{ pF}$.

For this test, we measured $\varepsilon(p, T)$ for argon up to 6 MPa on three isotherms using the ring and the rod capacitors simultaneously. Both capacitors were exposed to the same gas while they were in the same thermostated bath and were connected to the same pressure gage. Thus, this test was insensitive to impurities in the argon and to imperfect measurements of the temperature and pressure. Because the capacitances were measured nearly simultaneously, it was insensitive to possible drift of the capacitance standard within the bridge. This test was sensitive only to imperfections of the capacitors, the electrical cables and switches, and to the ratios determined by the capacitance bridge.

The values of $C_x(p, T)$ for both cross capacitors are shown on Figs. 4a and 4b. Figure 4c displays the ratios C_{rod}/C_{ring} computed at every
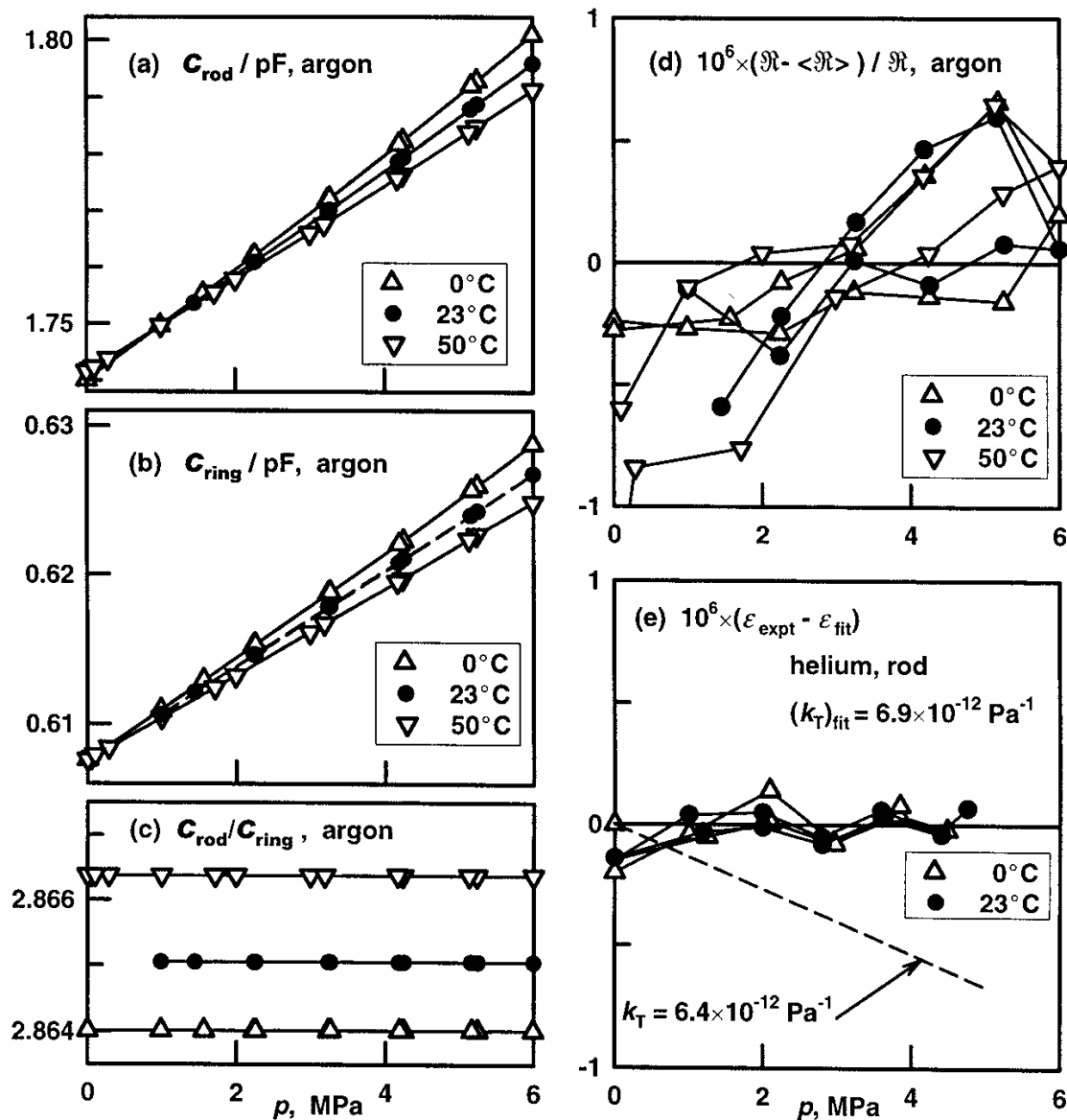
Fig. 4. Consistency of argon data taken with the ring and rod capacitors. (a) and (b): Capacitance of the two cross capacitors measured simultaneously as a function of temperature and argon pressure. (c) Ratios of the data from panels (a) and (b) at each value of (p, T). (d): Fractional deviations of the capacitance ratios from their mean values on each isotherm, after correction for the deformation of the capacitors with pressure and after multiplication by 10^6. By definition, the average deviation from the mean is zero; however, the standard deviation is 0.50×10^{-6}. If a linear pressure dependence is subtracted, the standard deviation is reduced to 0.33×10^{-6}. (e) Fractional deviations of the helium data from the fit that determined the compressibility of the rod capacitor $k_T = 6.9 \times 10^{-12}$ Pa^{-1}. If the literature value $k_T = 6.4 \times 10^{-12}$ Pa^{-1} had been used, the helium data would lie along the dashed curve.

value of (p, T) where C_x was measured. On the scale of Fig. 4c, the ratios C_{rod}/C_{ring} change with temperature, but the change with pressure is too small to see. The temperature dependence is that of the vacuum ratios $C_{rod}(0, T)/C_{ring}(0, T)$ and results from the difference between the thermal expansion of the steel rods and that of the Invar rings. Because the gas in both capacitors was identical whenever C_{rod}/C_{ring} was measured, the pressure independence was expected. We made a more revealing analysis of the data in Figs. 4a and 4b by assuming that both cross capacitors deform according to Eq. (4). At every value of (p, T), we computed the ratio $\Re(p, T)$ defined by

$$\Re(p, T) \equiv \frac{[C_{rod}(p, T)](1 + k_{T, rod} p/3)}{[C_{ring}(p, T)](1 + k_{T, ring} p/3)} \overset{?}{=} \frac{[\varepsilon_{expt} C_{rod}(0, T)]}{[\varepsilon_{expt} C_{ring}(0, T)]}. \tag{8}$$

We asked the question: is $\Re(p, T)$ independent of pressure, as expected from the right side of Eq. (8)? The answer is displayed in Fig. 4d. Figure 4d displays the fractional differences of $\Re(p, T)$ from its average value, $(\Re(p, T) - \langle\Re(p, T)\rangle)/\langle\Re(p, T)\rangle$, where the average value was computed separately on each isotherm. The standard deviation of the fractional differences is $\sigma = 0.50 \times 10^{-6}$. The fractional differences do have a small pressure dependence consistent with the linear equation: $\langle\varepsilon_{rod}\rangle - \langle\varepsilon_{ring}\rangle = (0.161 \pm 0.025) \times 10^{-6} \times (p/\text{MPa})$. Subtracting this dependence term reduces σ to 0.33×10^{-6}.

If the pressure dependence in Fig. 4d is attributed to imperfections of the capacitance bridge, it is equivalent to an error of 1 ppm of the capacitance change. Such an error is well within the manufacturer's specifications. If the pressure dependence in Fig. 4d is interpreted as a polarizability dependence, the slope is equivalent to $1.3 \times 10^{-4} \text{ cm}^3 \cdot \text{mol}^{-1}$ or $3 \times 10^{-5} A_\varepsilon$ for argon. Thus, the residual pressure dependence (an inconsistency) is comparable to the random uncertainties reported by MB when they determined A_ε by fitting $\varepsilon(p, T)$ data from the ring capacitor to Eq. (5). This inconsistency is smaller than the uncertainty of $\varepsilon(p, T)$ measurements made elsewhere under comparable conditions, and it is much smaller than the uncertainty of A_ε that results from the uncertainty of argon's equation of state used to convert $\varepsilon(p, T)$ to $\varepsilon(\rho, T)$.

We have five remarks concerning this consistency test. (1) The test has no adjustable parameters. (2) By choosing $k_{T, rod} = 6.3 \times 10^{-12} \text{ Pa}^{-1}$, we could force the inconsistency to vanish from Fig. 4d; however, an inconsistency of the same size but opposite sign would then appear in the helium calibration data in Fig. 4e. (The scales in Figs. 4d and 4e are identical.) (3) The test results are stable; The data in Fig. 4d were taken during a two-week-long interval. (4) We are unable to determine whether the inconsistency

results from imperfections of the ring capacitor, the rod capacitor, the capacitance bridge, cables, etc., or some combination of them. (5) The relative vertical positions of the isotherms in Fig. 4d are irrelevant; they were determined by the choice to subtract $\langle \Re(p, T) \rangle$ on each isotherm. Other constants could have been subtracted. A natural choice is to subtract the vacuum ratio $C_{rod}(0, T)/C_{ring}(0, T)$ on each isotherm. However, the vacuum measurements were particularly troublesome because $\tau_{thermal}$ was so large under vacuum. The average $\langle \Re(p, T) \rangle$ de-emphasizes the vacuum measurements.

It is interesting to notice that the isotherms on Fig. 4a cross near 1 MPa. A crossing at some pressure is inevitable because thermal expansion increases $C_{rod}(0, T)$ with temperature, while, on isobars, $\varepsilon(p, T) \times C_{rod}(0, T)$ decreases with temperature as does $\rho(p, T)$.

5. RESULTS

Our results for $\varepsilon(p, T)$ appear in Tables I to IV. In each column, the data from the ring capacitor are listed in the order in which they were taken. When computing $\varepsilon(p, T)$ using Eq. (4), we usually averaged the values of $C_{ring}(p = 0, T)$ from the beginning and the end of each measurement cycle. Because of averaging, either the first and the last entries for $100 \times (\varepsilon - 1)$ are both zero or they are equal with opposite signs.

Table I. Relative Dielectric Permittivity of Helium

$T = 29.3°C$		$T = 0.019°C$	
p (kPa)	$100(\varepsilon - 1)$	p (kPa)	$100(\varepsilon - 1)$
0.00	0.00000	0.00	0.00000
1060.15	0.06510	1029.97	0.07001
2297.72	0.14032	2268.93	0.15330
3312.50	0.20141	3281.89	0.22058
4059.24	0.24599	3937.39	0.26379
5124.92	0.30915	4837.64	0.32266
6247.38	0.37500	6205.02	0.41112
6996.60	0.41860	6988.96	0.46134
6088.77	0.36573	5568.82	0.37011
5258.85	0.31703	5140.49	0.34237
4281.08	0.25916	3919.66	0.26263
3261.41	0.19833	3014.24	0.20289
2252.06	0.13755	1985.11	0.13430
1258.42	0.07721	1047.49	0.07119
0.00	0.00000	0.00	0.00000

This accounts for the few, slightly negative, values of $100 \times (\varepsilon - 1)$. The tabulated pressures are the readings of the pressure transducer corrected for the hydrostatic head, corrected to an isotherm (see MB, Section 3.2), and corrected by a calibration function (see MB, Section 3.1). Because the calibration function was averaged over the transducer's hysteresis, the corrected pressures could be slightly negative at the end of a measurement cycle. This accounts for the few, slightly negative, pressures in the table.

Table II. Relative Dielectric Permittivity of Propane and Ethane

Propane

$T = 0.02°C$		$T = 22.5°C$		$T = 40.0°C$	
p (kPa)	$100(\varepsilon - 1)$	p (kPa)	$100(\varepsilon - 1)$	p (kPa)	$100(\varepsilon - 1)$
0.000	−0.00003	0.000	0.00000	0.000	0.00000
180.539	0.39796	217.382	0.44136	207.511	0.39438
266.028	0.59907	404.760	0.85287	399.244	0.78262
321.031	0.73356	553.944	1.20593	550.920	1.10875
375.356	0.87072	704.419	1.59017	703.931	1.45760
416.535	0.97776	815.959	1.89747	817.812	1.73222
377.933	0.87734	707.117	1.59743	704.647	1.45926
332.117	0.76126	556.333	1.21183	551.709	1.11052
287.461	0.65101	472.392	1.00992	452.173	0.89433
256.451	0.57614	399.934	0.84197	373.261	0.72853
−0.003	0.00003	0.004	0.00001	−0.003	−0.00003

Ethane

$T = 0.02°C$		$T = 22.5°C$		$T = 40.0°C$	
p (kPa)	$100(\varepsilon - 1)$	p (kPa)	$100(\varepsilon - 1)$	p (kPa)	$100(\varepsilon - 1)$
0.00	0.00003	0.00	0.00001	0.00	−0.00001
198.84	0.29925	292.48	0.40816	240.08	0.31391
658.70	1.04575	1292.26	1.98695	1060.64	1.47705
1013.27	1.68590	2087.05	3.53632	1704.55	2.51143
1366.42	2.39715	2883.58	5.56369	2351.67	3.69708
1721.04	3.21372	3483.16	7.76199	3002.94	5.09798
1986.58	3.92041	2916.52	5.66381	3489.01	6.34092
1737.01	3.25367	2109.30	3.58502	3022.02	5.14310
1377.98	2.42224	1322.09	2.03948	2370.63	3.73463
1040.17	1.73721	911.70	1.34752	1713.42	2.52657
787.99	1.27185	0.01	−0.00001	1062.28	1.47956
613.13	0.96794			735.49	0.99792
0.01	−0.00003			−0.01	0.00001

Table III. Relative Dielectric Permittivity at 29.3°C

Methane		Nitrogen		Carbon Dioxide		Argon		Oxygen	
p (kPa)	$100(\varepsilon-1)$	p (kPa)	$100(\varepsilon-1)$	p (kPa)	$100(\varepsilon-1)$	p (kPa)	$100(\varepsilon-1)$	p (kPa)	$100(\varepsilon-1)$
0.00	−0.00001	0.00	0.00000	0.00	0.00001	0.00	0.00000	0.00	0.00000
1008.18	0.80294	1008.76	0.52978	712.77	0.64989	750.79	0.37302	1014.93	0.48296
2273.85	1.85653	2272.76	1.19787	1609.72	1.55081	1744.80	0.87330	2257.79	1.08408
3266.37	2.71938	3255.85	1.71997	2310.86	2.33570	2521.28	1.26895	3257.64	1.57504
4276.46	3.63133	4015.49	2.12435	3023.01	3.22616	3317.53	1.67899	4237.88	2.06251
5241.38	4.53406	5026.19	2.66316	3730.75	4.23348	4102.37	2.08716	5246.21	2.56971
6252.83	5.51324	6244.33	3.31237	4455.90	5.44205	4895.75	2.50362	6238.43	3.07411
6997.49	6.25492	6988.17	3.70847	4987.24	6.49073	5488.95	2.81735	7000.90	3.46498
5902.55	5.17028	5941.75	3.15133	4355.55	5.26150	4831.79	2.46992	6145.83	3.02687
5140.08	4.43771	5139.12	2.72342	3668.26	4.13857	4116.14	2.09441	5073.92	2.48267
1075.12	0.85743	4987.80	2.64260	2974.04	3.16162	3324.41	1.68265	4256.00	2.07157
3243.04	2.69876	1974.13	1.03974	2239.80	2.25274	2506.50	1.26146	3260.61	1.57658
2257.01	1.84215	3251.56	1.71772	1596.95	1.53765	1741.95	0.87195	2262.78	1.08656
1257.78	1.00661	3999.70	2.11593	887.36	0.81765	947.82	0.47169	1257.54	0.59945
0.00	0.00001	3244.67	1.71409	0.00	−0.00001	0.00	0.00000	0.00	0.00000
		2269.70	1.19627						

Table IV. Relative Dielectric Permittivity at 0.019°C

Methane		Nitrogen		Carbon Dioxide		Argon		Oxygen	
p (kPa)	$100(\varepsilon-1)$	p (kPa)	$100(\varepsilon-1)$	p (kPa)	$100(\varepsilon-1)$	p (kPa)	$100(\varepsilon-1)$	p (kPa)	$100(\varepsilon-1)$
0.00	0.00001	0.00	−0.00004	0.00	0.00000	0.00	−0.00001	0.00	0.00000
999.49	0.88786	1011.42	0.58981	504.09	0.50844	991.90	0.54860	992.19	0.52454
2248.69	2.06910	2262.62	1.32918	1361.90	1.48089	2239.60	1.25587	2247.82	1.20511
3245.63	3.07381	3240.72	1.91355	2059.04	2.40850	3243.32	1.83844	3237.49	1.75449
4238.04	4.13272	4251.03	2.52181	2768.17	3.54860	4234.86	2.42573	4237.23	2.32082
5256.46	5.28276	5271.85	3.14005	3292.20	4.60399	5253.73	3.04062	5236.14	2.89760
6222.12	6.43719	6230.70	3.72303	2754.03	3.52329	6239.07	3.64584	6231.54	3.48267
6982.58	7.38857	6995.51	4.18873	2021.93	2.35526	6987.92	4.11223	6979.65	3.92881
5923.25	6.07363	5900.54	3.52219	1354.79	1.47234	6059.72	3.53495	6004.90	3.34864
4953.30	4.93400	5042.95	3.00129	666.10	0.68083	5152.12	2.97882	5008.19	2.76509
4080.18	3.96018	4046.89	2.39873	0.00	0.00000	4173.85	2.38932	4032.01	2.20371
3170.77	2.99632	3074.30	1.81390			3218.20	1.82387	3254.85	1.76426
2280.60	2.10037	2008.63	1.17843			2259.46	1.26736	2274.32	1.21971
1264.64	1.13174	995.65	0.58066			1257.76	0.69778	1247.24	0.66129
0.00	−0.00001	0.00	0.00004			−0.02	0.00001	0.00	0.00000

The tabulated results can be used as reference data to test the performance of systems, such as re-entrant resonators [10], designed to measure $\varepsilon(p, T)$. If the tests are made with helium, we recommend using the theoretical values of $\varepsilon(p, T)$, to the extent possible, as we did in Section 2.4.

When discussing our results, we included the MB data because they were acquired with the same instrument; for brevity, the MB data are not included in Tables I to IV.

5.1. Fitting $\varepsilon(\rho, T)$

In order to assess the internal consistency of the present data, we converted $\varepsilon(p, T)$ to $\varepsilon(\rho, T)$ because the density representation is far simpler. As shown in Section 6 later, $[\varepsilon(\rho, T) - 1]$ for methane can be represented to within $\pm 0.015\%$ of ρ using only 5 fitting parameters, even though the data range from the triple point to 1.7 times the critical temperature and from the dilute gas to the triple point density. An equally accurate representation of $\varepsilon(p, T)$ over the same range of conditions would have the full complexity of an accurate equation of state and would require on the order of 20 terms. (Some accurate equations of state have fewer than 20 terms; however, such equations have more parameters than terms because the exponents in the terms are parameters that were varied when the terms were selected.)

We converted $\varepsilon(p, T)$ to $\varepsilon(\rho, T)$ with a precision of six significant figures using the wide-range, equations of state embedded in NIST Standard Reference Database 23 [11]. However, the equations of state in NIST23 are inconsistent with simple representations of the present data for propane and ethane. In contrast, equations of state derived from speed of sound measurements in gaseous propane and ethane are consistent with the present data, and we recommend them for this purpose.

The $\varepsilon(\rho, T)$ data were fitted by functions that had, at most, four coefficients selected from the five coefficients $A_{\varepsilon, 273}$, b, c, A_τ, and q in the expression

$$(\varepsilon - 1)/(\varepsilon + 2) = A_{\varepsilon, 273}\, \rho(1 + b\rho + c\rho^2)$$

$$+ A_\tau \rho \left(\frac{T}{273.16\ \mathrm{K}} - 1 \right) + q\rho^2 \left(\frac{273.16\ \mathrm{K}}{T} - 1 \right) \qquad (9)$$

To reflect the uncertainties of the measurements, all the data, including the data near zero density, were weighted equally. Figures 5 to 7 display the deviations from Eq. (9) multiplied by 3×10^6. To construct these plots, we ignored the small (2% or less) variation of $(\varepsilon + 2)$; then, the ordinates are $10^6 \times (\varepsilon_{\mathrm{expt}} - \varepsilon_{\mathrm{fit}})$, which we abbreviate as $10^6 \Delta\varepsilon$.

5.2. Uncertainties

For the nearly ideal gases (helium, argon, nitrogen, oxygen, and methane), the fits are well behaved, and the three parameters $A_{\varepsilon, 273}$, A_τ, and b in Eq. (9) are of interest to theory. To discuss the uncertainties of our determinations of these parameters, we return to the expansion of the capacitance ratios in powers of $p/(RT)$, Eq. (7).

In effect, $A_{\varepsilon, 273}$ is determined by the relation $A_\varepsilon = RT/(3p)[C_x(p)/C_x(0) - 1] + k_T RT/9$. Because, the uncertainties of R and T are very small, it follows that the uncertainty of $A_{\varepsilon, 273}$ is the quadrature sum of three terms: $\delta \times A_{\varepsilon, 273}$, $10^{-6} A_{\varepsilon, 273}/(\varepsilon_{max} - 1)$, and $1.1 \times 10^{-4} \, cm^3 \cdot mol^{-1}$. In the first term, the factor $\delta \approx 3 \times 10^{-5}$ originates in the uncertainty of the pressure measurements. The second term $10^{-6} A_{\varepsilon, 273}/(\varepsilon_{max} - 1)$ originates in the uncertainty of the capacitance ratio measurements; the prefactor 10^{-6} is the result of our consistency check (Section 4) and ε_{max} is the maximum value of ε used in the fit. The third term, $1.1 \times 10^{-4} \, cm^3 \cdot mol^{-1}$, propagates from the uncertainty of k_T (Section 2.4). As the equation of state departs from that of an ideal gas, the higher terms in the pressure expansion become important. Then, the range of the data that determine $A_{\varepsilon, 273}$ must be restricted. In these cases (carbon dioxide and ethane) the term $10^{-6} A_{\varepsilon, 273}/(\varepsilon_{max} - 1)$ dominates the uncertainty of A_ε.

In effect, A_τ is determined by the difference between the values of A_ε on our two most widely separated isotherms (T_{high} and T_{low}). The uncertainty contributions from the pressure transducer and the bulk modulus of capacitor are correlated on both isotherms; thus, the uncertainty of A_τ is dominated by the uncertainty of the capacitance ratios on the two isotherms at $\sqrt{2} \times 10^{-6} A_{\varepsilon, 273}/[(\varepsilon_{max} - 1)(T_{high} - T_{low})]$.

In this work, the dielectric virial coefficient is determined by the second coefficient a_2 in Eq. (7), the expansion of the capacitance ratio in powers of $p/(RT)$. The term $(k_T RT/3)^2$ is always negligibly small. The terms B and A_ε are usually of the same order of magnitude and both are much larger than b. In this work we determine a_2 and A_ε very accurately and we implicitly take B from the literature when we select an equation of state. For argon, nitrogen, and methane, reliable values of B in the range 0 to 50°C from different laboratories are bracketed by ± 0.15, ± 0.2, and $\pm 0.35 \, cm^3 \cdot mol^{-1}$, respectively [12]. The uncertainty of b is dominated by the uncertainty of B.

5.3. Results for $\varepsilon(\rho, T)$

For argon and nitrogen, we used equations of state from Refs. 13 and 14, respectively, to convert $\varepsilon(p, T)$ to $\varepsilon(\rho, T)$. The values of $\varepsilon(\rho, T)$ were fit to

Eq. (9) using the two parameters, A_ε and b, as indicated on Figs. 5a and 5b. The remaining parameters were set equal to zero. The standard deviations of the fits were approximately 1 ppm of $\Delta\varepsilon$. (1 ppm $\equiv$ 1 part in 10^6). This is approximately twice the standard deviation found during the comparison of the ring and rod capacitors using argon (Fig. 4d). Thus, these deviations probably represent the limitations of the data, and not limitations of the equation of state. The resulting values of A_ε and b and their uncertainties are listed in Table V. For both argon and nitrogen, the fitting contributed only 0.015 $cm^3 \cdot mol^{-1}$ to the uncertainty of b. A much larger contribution to the uncertainty of b is hidden in the conversion from pressure to density. [In effect, we measure a_1 and a_2 in Eq. (7) and b is determined *via* subtraction: $b \approx B - A_\varepsilon + a_2/(3A_\varepsilon)$.] For argon and nitrogen, reliable values of B in the range 0 to 50°C from different laboratories are bounded by ± 0.15 and ± 0.2 $cm^3 \cdot mol^{-1}$, respectively [12]. Thus, the uncertainty of b in this work is dominated by the uncertainty of B.

For oxygen, we used the equation of state from Ref. 15 to convert $\varepsilon(p, T)$ to $\varepsilon(\rho, T)$. The values of $\varepsilon(\rho, T)$ were fit to Eq. (9) using two nonzero parameters, A_ε and b, as indicated on Fig. 5c. In Fig. 5c, the deviations

Table V. Coefficients for Eq. (9), the Polynomial Expansion of $(\varepsilon-1)/(\varepsilon+2)$ as a Function of ρ and T. (For the more satisfactory fits, the uncertainty of the last two digits of each coefficient is shown in parentheses. The uncertainty of $A_{\varepsilon, 273}$ from the elastic properties of the capacitor is 1.1×10^{-4} $cm^3 \cdot mol^{-1}$. The uncertainties of b, c, A_τ, and q from the equations of state are much larger than the indicated uncertainties.)

Gas	Eq. of state ref.	$A_{\varepsilon, 273}$ $cm^3 \cdot mol^{-1}$	b $cm^3 \cdot mol^{-1}$	c $cm^6 \cdot mol^{-2}$	A_τ $cm^3 \cdot mol^{-1}$	q $cm^6 \cdot mol^{-2}$	$10^6 \times \sigma$
Ar	[13]	4.14203 (19)	0.281 (15)				0.98
N_2	[14]	4.38782 (18)	0.399 (14)				0.91
N_2	[14]	4.38748 (15)	0.417 (11)		0.00170 (30)		0.69
O_2	[15]	3.95945	−0.113				1.86
O_2	[15]	3.95875 (09)	−0.077 (07)		0.00648 (27)		0.39
CH_4	[19]	6.54787	0.981				2.95
CH_4	[19]	6.54467 (31)	1.250 (34)	−44.7 (68)	0.00622 (36)		0.86
C_3H_8	[22]	15.8536	3.360				3.0
C_3H_8	[23]	15.8527 (22)	6.27 (35)				1.20
CO_2	[26]	7.3797	6.230		0		12.6
CO_2	[26]	7.34590 (63)	10.023 (80)	−557. (20)		114.21 (61)	1.3
C_2H_6	[24]	11.16041	1.468		0.031		2.7
C_2H_6[a]	[25]	11.15757 (60)	1.759 (47)		0.019 (17)		1.1
C_2H_6	[24]	11.15183	1.41 (11)		0.046		2.8
C_2H_6[a]	[24]	11.15722 (74)	1.328 (73)		0.0280 (26)		0.95

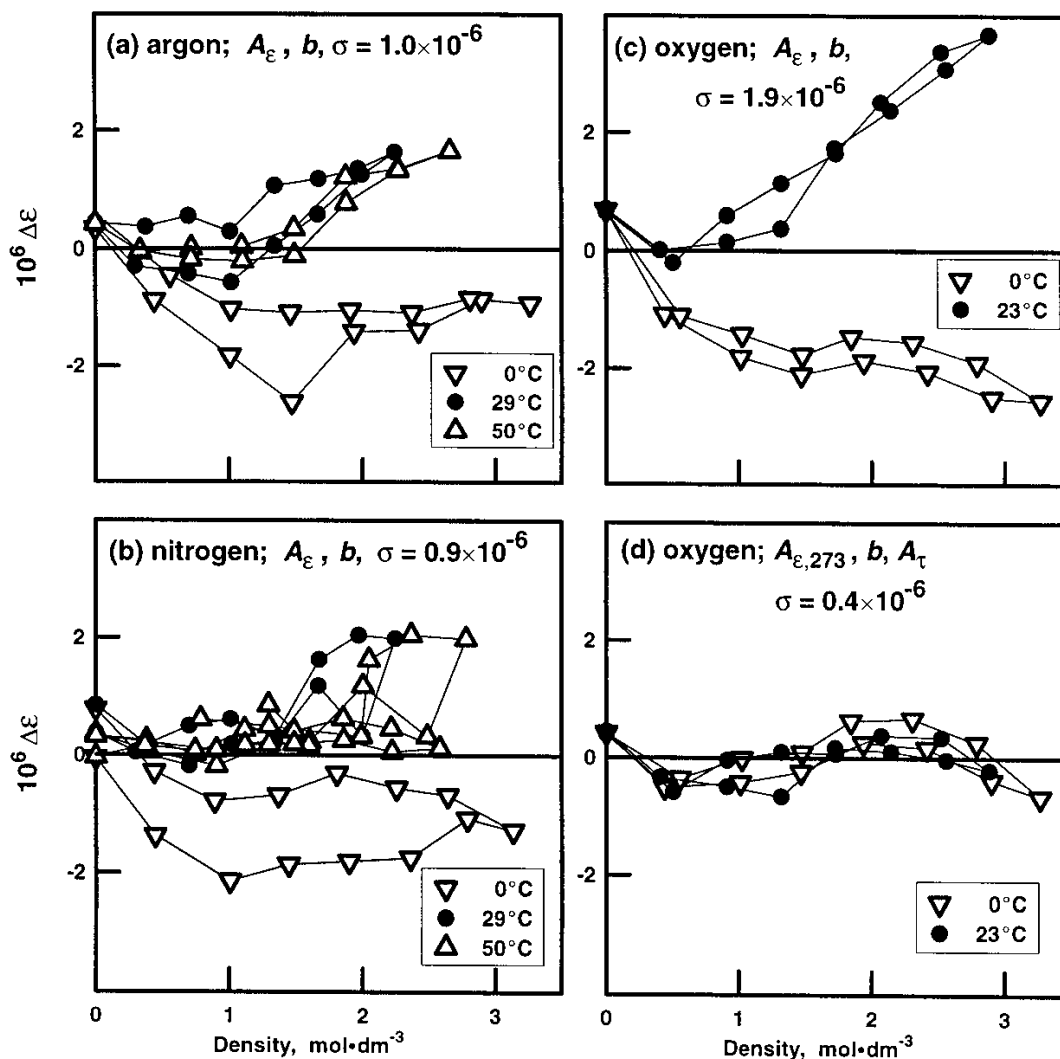[a] Fit to data up to 1.2 $mol \cdot dm^{-1}$ only.

Fig. 5. Deviations of $\varepsilon(p, T)$ data from a linear function of density for (a) argon, (b) nitrogen, and (c) oxygen. The oxygen data in (d) are the same as in (c); however, a third parameter [A_τ in Eq. (7)] was also fitted. The fitted parameters are in Table V.

of the two oxygen isotherms are approximately linear in density and have opposite slopes. This is evidence that A_ε is temperature-dependent. To allow for this, the third parameter A_τ was added to the fit. The value $A_\tau = 0.0065 \text{ cm}^3 \cdot \text{mol}^{-1}$ significantly reduced the deviations as shown in Fig. 5d. We also considered the possibility that $A_\tau \neq 0$ in nitrogen. As shown in Table V, the value $A_\tau = 0.0017 \text{ cm}^3 \cdot \text{mol}^{-1}$ lowered the standard deviation of the fit for nitrogen from 0.91 to 0.69. Anharmonic vibration and molecular rotation ("centrifugal stretching") both lead to increases of A_ε with temperature. For oxygen, vibration is characterized by the temperature $\theta \approx 2228$ K; for nitrogen, $\theta \approx 3336$ K. At the temperatures in this work, nearly all the oxygen and nitrogen are in their ground states; thus, one expects the vibrational contributions to be very small [16]. The

rotational contribution to A_ε is proportional to the temperature; however, its values for nitrogen and oxygen are likely to be similar [17].

Younglove [18] also measured the dielectric constant of oxygen and fitted his data with a function that is equivalent to Eq. (9) with the parameters A_ε, b , c, and A_τ. He found $A_\tau = -0.0059 \, \text{cm}^3 \cdot \text{mol}^{-1}$, which is inconsistent with the present value $A_\tau = (0.0065 \pm 0.0003) \, \text{cm}^3 \cdot \text{mol}^{-1}$. The inconsistency is not surprising because Younglove's linear term was determined mostly by his compressed liquid data in the ranges $100 \, \text{K} \leqslant T \leqslant 140 \, \text{K}$ and $25 \, \text{mol} \cdot \text{dm}^{-3} \leqslant \rho \leqslant 35 \, \text{mol} \cdot \text{dm}^{-3}$, while all of the present data are at much lower densities: $\rho \leqslant 3 \, \text{mol} \cdot \text{dm}^{-3}$. It is probable that Younglove's value of A_τ is fitting either an average temperature-dependence of higher dielectric virial coefficients or a temperature-dependence that was not included in the equation of state.

Figures 6a and 6b display the deviations of the present $\varepsilon(\rho, T)$ data for methane from two- and four-parameter fits, respectively, where we have used the equation of state from Ref. 19. All four parameters are statistically significant; the standard deviation of the four-parameter fit for methane is comparable to the standard deviations of the two-parameter fits for argon and nitrogen. From our four-parameter fit, we found $A_\tau \approx 6 \times 10^{-3} \, \text{cm}^3 \cdot \text{mol}^{-1}$; when we added the 5th parameter b_τ to the fit, we found $A_\tau \approx 11 \times 10^{-3} \, \text{cm}^3 \cdot \text{mol}^{-1}$. These values bracket the value $A_\tau \approx 8.4 \times 10^{-3} \, \text{cm}^3 \cdot \text{mol}^{-1}$ calculated by Wong et al. [17] at optical frequencies. All three values are smaller than the value $A_\tau \approx 17 \times 10^{-3} \, \text{cm}^3 \cdot \text{mol}^{-1}$ measured by Bose et al. [20].

In Figs. 6c and 6d, we consider propane. Our propane data fall in the range $273 \, \text{K} \leqslant T \leqslant 313 \, \text{K}$ where propane has a comparatively low vapor pressure. Thus, the data were limited to the range $\rho \leqslant 0.4 \, \text{mol} \cdot \text{dm}^{-3}$, which is only $1/8$ of the density range available for the other gases considered here. Furthermore, propane has a small dipole moment $\mu = (0.0848 \pm 0.0005) \, D$ that is well-known from careful, redundant, microwave measurements [21]. Between 273 and 323 K, the dipolar contribution to the molar polarizability, $(4\pi N_A \mu^2)/(9k_B T)$, decreases from 0.160 to 0.140 $\text{cm}^3 \cdot \text{mol}^{-1}$ and it has an uncertainty of only 1.2% of its value. With these considerations in mind, we fit the propane data by the equation

$$\left(\frac{\varepsilon - 1}{\varepsilon + 2}\right) - \rho \, \frac{4\pi N_A \mu^2}{9k_B T} = \rho A_\varepsilon (1 + b\rho), \tag{10}$$

where the only fitting parameters were A_ε and b. We used two different equations of state to convert $\varepsilon(p, T)$ to $\varepsilon(\rho, T)$. The deviations in Fig. 6c are based on the equation of state of Younglove and Ely [22]; the deviations in Fig. 6d are based on the virial equation of state constructed by
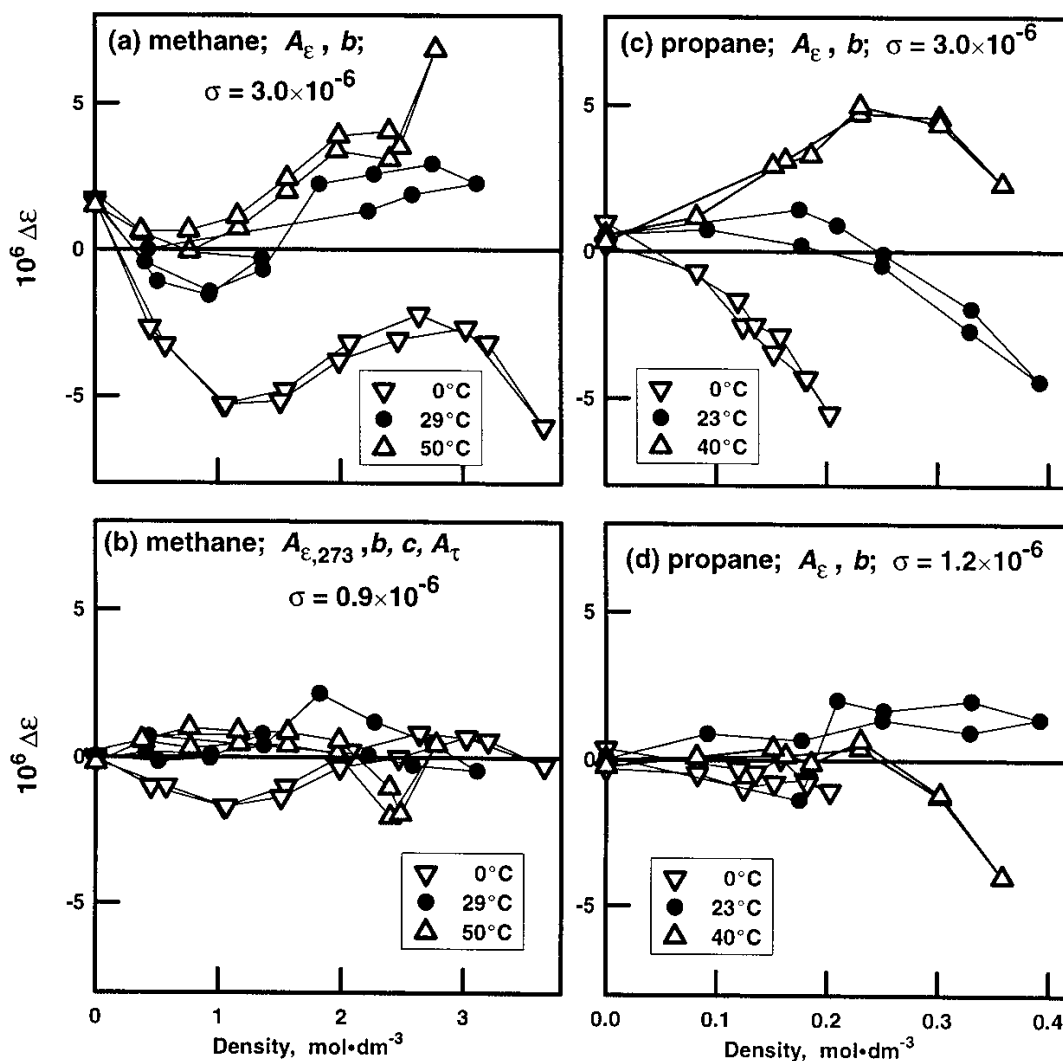
Fig. 6. Deviations of $\varepsilon(p, T)$ data from Eq. (7). (a) Two-parameter fit for methane. (b) Four-parameter fit for methane. (c) Two-parameter fit for propane using the equation of state from Ref. 19. (d) Two-parameter fit for propane using equation of state from Ref. 22. The equation of state from Ref. 23 is more consistent with the present data.

Trusler [23]. The present data are more nearly consistent with Trusler's equation of state. This is not surprising because Trusler's equation of state was derived from very accurate speed-of-sound data at low densities. Such data lead to very accurate virial coefficients. In contrast, Younglove and Ely correlated diverse measurements over a much wider range of conditions.

Carbon dioxide and ethane are considered in Fig. 7. Both carbon dioxide and ethane were studied near their critical temperatures T_c but well below their critical densities ρ_c, where any critical anomaly is negligible. (For CO_2, $0.90 < T/T_c < 1.06$ and $\rho/\rho_c < 0.26$; for C_2H_6, $0.89 < T/T_c < 1.03$ and $\rho/\rho_c < 0.32$.) For ethane, Table V includes results using two equations of state: one is the wide-range equation of state recommended
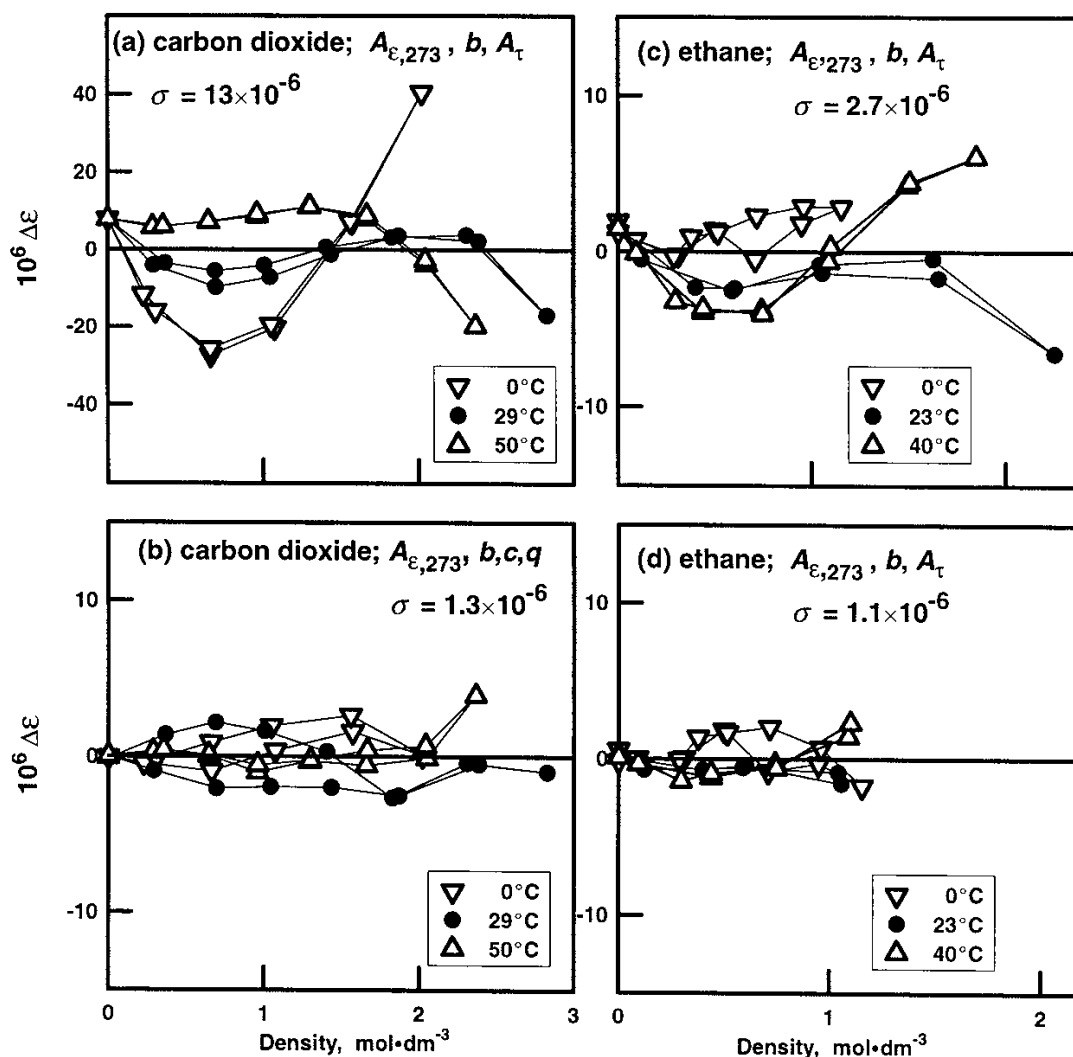
Fig. 7. Deviations of $\varepsilon(p, T)$ data from Eq. (7). (a) Three-parameter fit for carbon dioxide. (b) Five-parameter fit for carbon dioxide. (c) Three-parameter fit for ethane. (d) Three-parameter fit for the lowest-density data for ethane.

by REFPROP that was published by Friend et al. [24] and the other was based on gas-phase speed-of-sound data by Estrada-Alexanders and Trusler [25]. As was the case for propane, the equation of state based on gas-phase speed-of-sound data is more nearly consistent with the present gas-phase data. Three parameters fit the $\varepsilon(\rho, T)$ data for ethane (Fig. 7c) as well as three parameters fit methane and almost as well as they fit the data for argon, nitrogen, and oxygen. In Fig. 7d, we display the deviations from a three-parameter fit to only the low-density data for C_2H_6. This fit provides our best estimate for A_τ for ethane.

For carbon dioxide, we used the equation of state from Ref. 26, as recommended by REFPROP [11]. The standard deviation of the three-parameter fit for CO_2 is a factor of 5 larger than that for the corresponding

fit for C_2H_6. This is not surprising because CO_2 is known [27] to have a large quadrupole moment which leads to a temperature dependence of second dielectric virial coefficient b that is proportional to $1/T$. We allowed for the quadrupole moment by adding to the fit the fourth term: $q\rho^2(273.16\,\text{K}/T-1)$. Furthermore, we found that a temperature-dependent A_ε was much less significant than a ρ^3 term. Thus, a fit with the four parameters A_ε, b, c, and q in Eq. (9) led to the acceptable deviations shown in Fig. 7b. (Note: our CO_2 data are less precise than the C_2H_6 data because the CO_2 data were obtained using the older thermostated bath.) The value of q resulting from the fit is consistent with the temperature dependence of $B_\varepsilon = A_\varepsilon b$ measured by Bose and Cole [27] using an expansion technique. They report B_ε decreases by (6.9 ± 1.3) cm$^6\cdot$mol^{-2} between 29.4 and 49.7°C; our value for the decrease is 6.5 cm$^6\cdot$mol^{-2}.

6. COMPARISON WITH RESULTS FROM LITERATURE

Moldover and Buckley made extensive comparisons of their results with previously published results for helium, argon, nitrogen, methane, and carbon dioxide. Except for methane, they had to compare values of A_ε, b, and c instead of raw $\varepsilon(p, T)$ data, because the raw data were not available. They concluded that, in most cases, their values of A_ε were consistent with, but more accurate than, previously published values of A_ε. Also, their values of b were consistent with previously published values; however, their values of b were probably less accurate than those published values that were obtained using expansion methods, because expansion methods are only weakly sensitive to the uncertainties of the equations of state. We agree with these conclusions and shall not repeat their comparisons for the derived quantities A_ε, b, and c.

Recently, Ewing and Royal [28] reported new measurements of $\varepsilon(p)$, at 300 K for nitrogen at pressures up to 4 MPa. From their data, they deduced the values $A_\varepsilon = (4.3921\pm0.0019)$ cm$^3\cdot$mol^{-1} and $b = (0.45\pm0.39)$ cm$^3\cdot$mol^{-1}. Their value of A_ε differs from our value $A_\varepsilon = (4.3878\pm0.0009)$ cm$^3\cdot$mol^{-1} by only (0.0043 ± 0.0021) cm$^3\cdot$mol^{-1} where our uncertainty is from the two-parameter fit in Table V. The error from the fit must be augmented by the three contributions to the uncertainty of A_ε discussed in Section 5.2. For nitrogen they are: 1.3×10^{-4} cm$^3\cdot$mol^{-1} from pressure measurements, 1.1×10^{-4} cm$^3\cdot$mol^{-1} from capacitance measurements, and 1.1×10^{-4} cm$^3\cdot$mol^{-1} from the deformation of the ring capacitor under pressure. Thus, the known uncertainties are too small to explain the small inconsistency.

For methane, oxygen, and ethane, we are able to make new comparisons of our raw $\varepsilon(p, T)$ data with values from the literature. These follow.

6.1. Methane

In Fig. 8, we plot the molar polarizability $\wp = [(\varepsilon-1)/(\varepsilon+2)]/\rho$ for methane as a function of ρ along isotherms. In these variables, $\varepsilon(p, T)$ data spanning very wide ranges of temperature and pressure nearly collapse onto a single, smooth, function of the density. One can extrapolate $\wp(\rho, T)$ to $\rho = 0$ and read A_ε off the plot. These features facilitate comparisons without fitting. However, when plotted in these variables, the uncertainty of the ordinate diverges in proportion to $1/\rho$ as $\rho \to 0$. Also, except in the limit of zero density, the comparisons of data on different isotherms are subject to uncertainties from the equation of state. To prepare Fig. 8, we converted the data from Straty and Goodwin [29] to the ITS-90 and we calculated the densities for *all* the data using the equation of state from Ref. 19 as implemented in Ref. 11.

In Fig. 8, the values of $\wp(\rho, T)$ from Straty and Goodwin [29] lie consistently 0.11 to 0.17% below the present values. The difference is
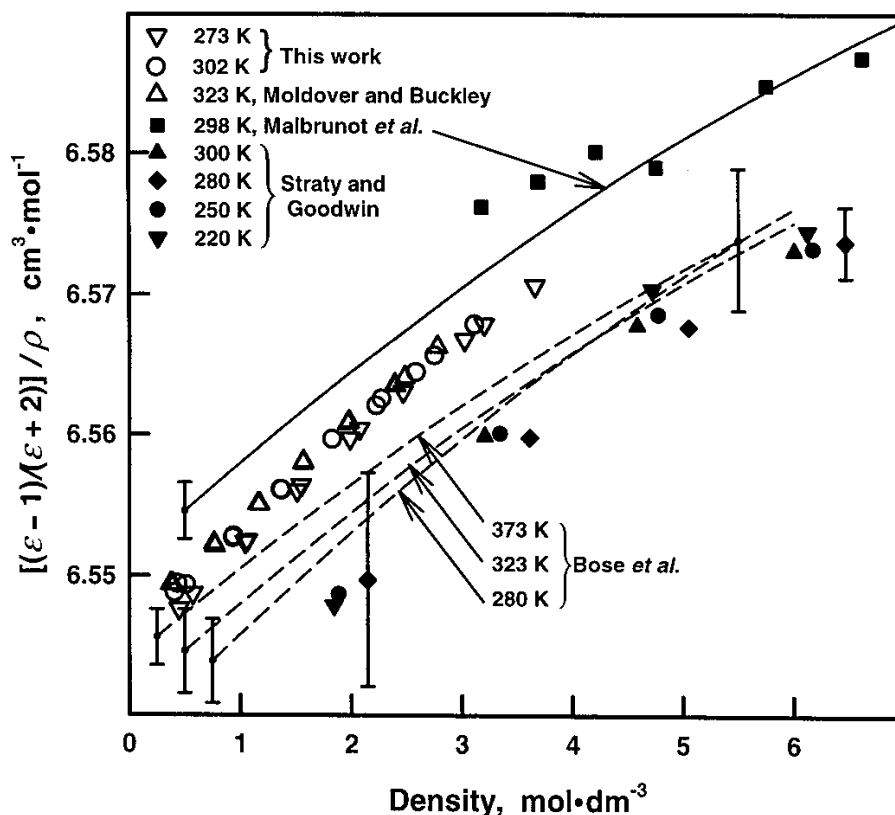

Fig. 8. Comparison of methane results from various sources. The plotted symbols were calculated using the equation of state from Ref. 19 and the $\varepsilon(p, T)$ data from this work, Moldover and Buckley [1], Straty and Goodwin [29], and Malbrunot et al. [30]. The curves represent Eq. (2) using the values of A_ε, b, and c from Bose et al. [20] and Malbrunot et al. [30].

acceptable; Straty and Goodwin designed their apparatus to operate at much higher densities and pressures (up to $28 \, \text{mol} \cdot \text{dm}^{-3}$ at 34 MPa) than we did. They estimated the uncertainty of their results for the polarizability was $\pm 0.15\%$ at low densities and 0.1% at higher densities. Their estimated uncertainties are illustrated by two error bars on their 280 K data in Fig. 8.

Figure 8 shows the low density data of Malbrunot et al. [30] and the curve that they fitted to their data, which extend to $33 \, \text{mol} \cdot \text{dm}^{-3}$ at 710 MPa. The error bar attached to the low-density end of their curve is the uncertainty they attributed to A_ε, namely, $\pm 0.002 \, \text{cm}^3 \cdot \text{mol}^{-1}$. The present data for methane are bracketed by the curve of Malbrunot et al. and by the data of Straty and Goodwin. In the worst case (the lowest density), the uncertainty of the present data corresponds to $\pm 0.0008 \, \text{cm}^3 \cdot \text{mol}^{-1}$ and this is smaller than the plotted squares. We believe that A_ε (which is the zero-pressure intercept of the data on Fig. 6) is more accurately determined by the present data than by the data from the literature.

For methane, Bose et al. [20] used an expansion method to determine values of A_ε, b, and c on the three isotherms: 280, 323, and 373 K. We used their tabulated values to plot three smooth curves labeled "Bose et al." in Fig. 8. We varied A_ε, b, and c within their uncertainties to obtain the error bars that are attached to the ends of these curves. (According to Malbrunot et al. [30] these error bars may be too small.) The three curves have a small temperature dependence at low densities that the authors attributed to real temperature dependences of A_ε, and b [20]. These trends appear in our data as well, as discussed in Section 5.3. In Fig. 8, the slope of our data is steeper than the curves representing the results of Bose et al. and Malbrunot et al. However, all our points plotted in Fig. 8 relied upon the equation of state. Because the equation of state contributed an uncertainty of approximately $0.35 \, \text{cm}^3 \cdot \text{mol}^{-1}$ to our value of b, our value is consistent with the literature for methane; however, our uncertainty is larger than the uncertainties claimed by Malbrunot et al. and by Bose et al.

6.2. Ethane and Oxygen

Figure 9 compares the present data for oxygen with the data from Younglove [18]. The data overlap, within their scatter.

Figure 9 also compares the present data for ethane with the extensive data of Weber [31]. Again the agreement is very good. For this wide-ranging comparison, we used the equation of state of Friend et al. [24]. The downward curvature of the present data at 273 K on Fig. 9 is a consequence of the equation of state; it does not occur in Fig. 7c, where we have used the equation of state of Estrada-Alexanders and Trusler [25].
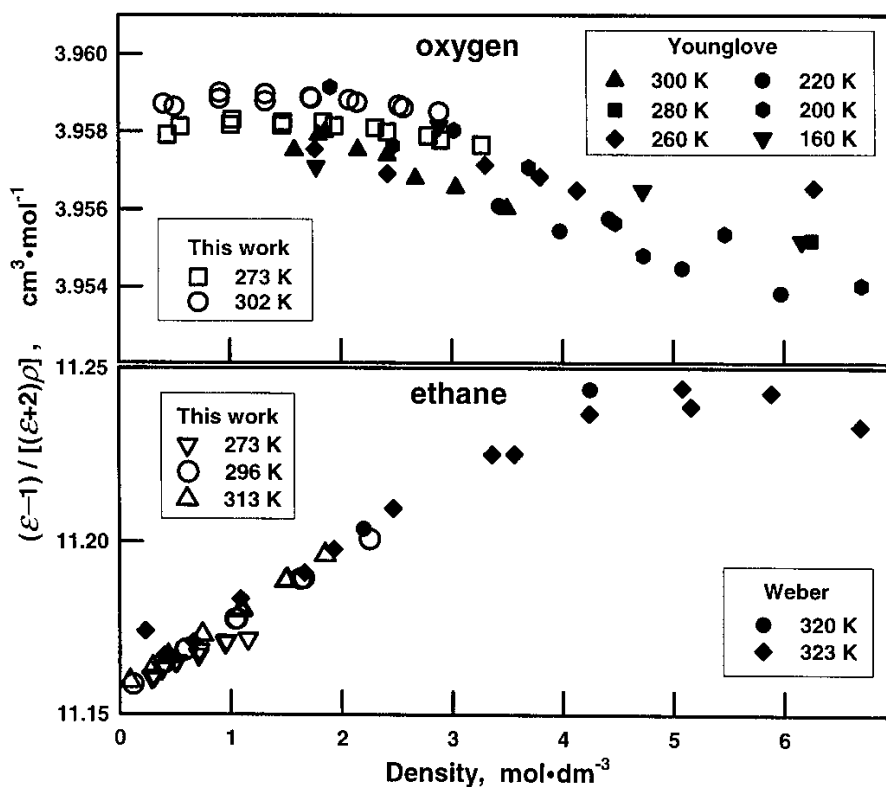
Fig. 9. Comparison of oxygen and ethane results with data from the literature. Oxygen: The open symbols represent the present data; the filled symbols represent the data of Younglove [18]. The values of $(\varepsilon-1)/[(\varepsilon+2)\,\rho]$ were calculated using the equation of state from Ref. 15. Ethane: The open symbols represent the present data; the filled symbols represent the data of Weber [31]. The values of $(\varepsilon-1)/[(\varepsilon+2)\,\rho]$ were calculated using the equation of state from Ref. 24.

ACKNOWLEDGMENT

We thank Dr. Allan Harvey of the Physical and Chemical Properties Division of NIST for continuing interest and valuable suggestions. We thank Dr. Andrés Estrada-Alexanders for assistance in using equations of state deduced from the speed of sound.

REFERENCES

1. M. R. Moldover and T. J. Buckley, *Int. J. Thermophys.* **22**:859 (2001).
2. M. Jaeschke, *Thermochimica Acta* **382**:37 (2002).
3. D. G. Lampard and R. D. Cutkosky, *Proc. Inst. Elect. Eng. (London)* **106**, pt. B mono. 351M (Jan. 1960).
4. J. Q. Shields, *IEEE Trans. Instrum. Meas.* **IM-21**:365 (1972); *IEEE Trans. Instrum. Meas.* **IM-27**:464 (1978).
5. A. M. Thompson and D. G. Lampard, *Nature (London)* **177**:888 (1956).
6. D. B. Lampard, *Proc. I.E.E., Monograph H, 216M* **104C**:271 (1957).

7. D. Makow and J. B. Campbell, *Metrologia* **8**:148 (1972); J. B. Campbell and D. Makow, *J. Comput. Phys.* **12**:137 (1973).
8. W. Chr. Heerens, B. Cuperus, and R. Hommes, *Delft Progress Report* **4**:67 (1979).
9. T. J. Buckley, J. Hamelin, and M. R. Moldover, *Rev. Sci. Instrum.* **71**:2914 (2000).
10. J. O. Hamlin, J. B. Mehl, and M. R. Moldover, *Rev. Sci. Instrum.* **69**:255 (1998).
11. E. W. Lemmon, M. O. McLinden, and M. L. Huber, *NIST Standard Reference Database 23, Reference Fluid Thermodynamic and Transport Properties-REFPROP, Version 7.0*, National Institute of Standards and Technology, Standard Reference Data Program, Gaithersburg, Maryland (2002).
12. J. P. M. Trusler, W. A. Wakeham, and M. P. Zarari, *Mol. Phys.* **90**:695 (1997).
13. Ch. Tegeler, R. Span, and W. Wagner, *J. Phys. Chem. Ref. Data* **28**:779 (1999).
14. R. Span, E. W. Lemmon, R. T Jacobsen, W. Wagner, and A. Yokozeki, *J. Phys. Chem. Ref. Data* **29**:1361 (2000).
15. R. Schmidt and W. Wagner, *Fluid Phase Equilib.* **19**:175 (1985), also published in: R. B. Stewart, R. T Jacobsen, and W. Wagner, *J. Phys. Chem. Ref. Data* **20**:917 (1991).
16. J. E. Mayer and M. G. Mayer, *Statistical Mechanics* (John Wiley, New York, 1940), p. 468.
17. A. T. Wong, G. B. Bacskay, N. S. Hush, and M. P. Bogaard, *Molec. Phys.* **74**:1037 (1991).
18. B. A. Younglove, *J. Res. Natl. Bureau Stand.* **76A**:37 (1972)
19. U. Setzmann and W. Wagner, *J. Phys. Chem. Ref. Data* **20**:1061 (1991).
20. T. K. Bose, J. S. Sochanski, and R. H. Cole, *J. Chem. Phys.* **57**:3592 (1972).
21. J. S. Meunter and V. W. Laurie, *J. Chem. Phys.* **45**:855 (1966).
22. B. A. Younglove and J. F. Ely, *J. Phys. Chem. Ref. Data* **16**:577 (1987).
23. J. P. M. Trusler, *Int. J. Thermophys.* **18**:635 (1997).
24. D. G. Friend, H. Ingham, and J. F. Ely, *J. Phys. Chem. Ref. Data* **20**:275 (1991).
25. A. F. Estrada-Alexanders and J. P. M Trusler, *J. Chem. Thermodynam.* **29**:991 (1997).
26. R. Span, and W. Wagner, *J. Phys. Chem. Ref. Data* **25**:1509, (1996).
27. T. K. Bose and R. H. Cole, *J. Chem. Phys.* **52**:140 (1970).
28. M. B. Ewing and D. D. Royal, *J. Chem. Thermodyanam.* **34**:1073 (2002).
29. G. C. Straty and R. D. Goodwin, *Cryogenics* **13**:712 (1973).
30. P. Malbrunot, J. Vermesse, D. Vidal, T. K. Bose, A. Hourri, and J. M. St-Arnaud, *Fluid Phase Equilib.* **96**:173 (1994).
31. L. A. Weber, *J. Chem. Phys.* **65**:446 (1976).